ROYAL SOCIETY
OF CHEMISTRY

PAPER
Andrew J. Musser, Helen Tran *et al.*
Impact of imine bonds on the electronic properties of
degradable carotenoid-based conjugated polymers

15 YEARS
ANNIVERSARY

Check for updates

Impact of imine bonds on the electronic properties of degradable carotenoid-based conjugated polymers†

Azalea Uva, [ID] [a] Yaejin Kim,[b] Sofia Michailovich,[a] Nathan S. Y. Hsu, [ID] [a] David C. Bain,[b] Shine H. Huang, [ID] [a] Andrew J. Musser [ID] *[b] and Helen Tran [ID] *[a,c,d]

Carotenoids are suitable building blocks for degradable π-conjugated polymers due to their intrinsic single-molecule conductance and well-documented degradation pathways. Previously, we reported a carotenoid-based polymer, p(CP-hexyl), which incorporated a cleavable imine linker enabling degradation *via* acid hydrolysis or sunlight; however, there was limited insight into its electronic properties. In this current study, we compare the optoelectronic and photophysical properties of p(CP-hexyl) with a structural analog, caro-PPV, which replaces the imine bonds with vinylene groups, to improve charge transport while maintaining degradability. Ultraviolet−visible spectroscopy, density functional theory, and transient absorption spectroscopy provided a comprehensive understanding of these polymers' optoelectronic properties. Further, chemical doping and oxidative degradation were evaluated using $FeCl_3$ and trifluoroacetic acid, unveiling differences in radical formation and degradation mechanisms for both carotenoid-based polymers. Lastly, charge carrier mobility measurements in organic field-effect transistors unveiled caro-PPV's superior semiconductor performance, with mobilities 10^3–10^4 times greater than p(CP-hexyl). These findings highlight the potential of carotenoid monomers in the design of π-conjugated polymers for degradable electronics.

Introduction

Conjugated polymers can be designed to impart stretchability,[1–3] thermal conductivity,[4,5] or degradability[6–8] through synthetic modifications at the monomeric level. Imparting degradability through the introduction of site-specific cleavable linkers in conjugated polymers is of notable interest, particularly for degradable electronics (*i.e.*, short-term applications or handling device obsolescence). Imine bonds are often introduced because they retain π-conjugation along a polymer backbone and are readily hydrolysed under acidic conditions. As such, numerous imine-bearing conjugated polymers, also known as poly(azomethine)s, have been synthesized to achieve recyclability,[9–11] understand degradation mechanisms,[12–14] and increase semiconducting performance in organic field-effect transistors (OFETs).[15,16] While reported literature focuses on the synthesis of degradable conjugated polymers, there is potential to simultaneously optimize electronic properties and degradability, paving the way for more efficient use of these materials as semiconductors in degradable electronics.

Towards designing with both electronic properties and degradability in mind, we previously reported a biobased degradable poly(azomethine)[17] (Fig. 1a) made from 2,7-dimethyl-2,4,6-octatrienedial (referred to as C10 dialdehyde), a carotenoid molecule obtained from the oxidative degradation of β-carotene.[18] β-Carotene derivatives have moderate single-molecule conductance[19–21] and well-documented degradation pathways in nature,[22–24] making them suitable as bioinspired alternatives to conventional π-conjugated building blocks. Our carotenoid-based poly(azomethine), termed p(CP-hexyl), degraded under two distinct conditions: imine hydrolysis and sunlight-mediated oxidation. Importantly, C10 dialdehyde was identified as one of the major degradation byproducts. While we successfully demonstrated the degradability of p(CP-hexyl), there was limited insight into the electronic properties, neces-

[a]Dept. of Chemistry, University of Toronto, Toronto, ON, M5S 3H6, Canada. E-mail: tran@utoronto.ca
[b]Dept. of Chemistry and Chemical Biology, Cornell University, Ithaca, NY, 14853, USA. E-mail: ajm557@cornell.edu
[c]Dept. of Chemical Engineering, University of Toronto, Toronto, ON, M5S 3H6, Canada
[d]Acceleration Consortium, University of Toronto, Toronto, ON, M5S 3H6, Canada

Fig. 1 Synthesis, chemical structures, and DFT models for carotenoid-based polymers. (a) Previously, we reported the synthesis of p(CP-hexyl), a carotenoid-based polymer produced through an imine polycondensation. Polymerization time was optimized in this study to yield lower molecular weight polymers. Right: image of p(CP-hexyl) as a red polymer. (b) Highest occupied molecular orbitals (HOMO) and lowest unoccupied molecular orbitals (LUMO) structures of p(CP-hexyl) obtained through density functional theory (DFT). (c) Imine model compound and corresponding HOMO–LUMO structures obtained from DFT. (d) In this work, we synthesized a new carotenoid-based polymer, termed caro-PPV, *via* Horner–Wadsworth–Emmons (HWE) polymerization. Right: image of caro-PPV as a red-brown polymer. (e) HOMO and LUMO structures of caro-PPV obtained from DFT. (f) Non-imine model compound and corresponding HOMO–LUMO structures obtained from DFT.

sitating further studies to determine its viability in electronic devices.

In this study, we evaluate the impact of imine bonds on the electronic properties of p(CP-hexyl). This investigation was inspired by a previous study by Bao and coworkers,[25] which found that imine-containing conjugated polymers exhibited similar, albeit slightly lower, charge carrier mobilities compared to their non-imine counterparts. To probe the direct effect of the imine bond in our system, we designed a new carotenoid-based polymer for which we termed caro-PPV (Fig. 1d) due to its similarity to poly(*p*-phenylene vinylene) (PPV), a well-studied organic conjugated polymer known for its conductive properties.[26–28] Caro-PPV bears structural similarity to p(CP-hexyl) with the difference being the substitution of the imine bonds with carbon–carbon double bonds (*i.e.* vinylene groups). Although a site-specific cleavable linker is absent in

caro-PPV, we hypothesized that it would be susceptible to degradation *via* oxidation, analogous to carotenoids in nature.[29–31] Therefore, our study not only investigates the effect of the imine bond on electronic properties, but also the broader degradation behaviours of carotenoid-based polymers. We report the optoelectronic properties and degradation of carotenoid-based polymers, p(CP-hexyl) and caro-PPV, characterized *via* ultraviolet-visible (UV-Vis) spectroscopy, gel permeation chromatography (GPC), nuclear magnetic resonance (NMR) and transient absorption (TA) spectroscopy. Additionally, we used density functional theory (DFT) and time-dependent DFT (TDDFT) to probe conformational changes that arise as a direct result of the imine bond (Fig. 1b and e). Model compounds (Fig. 1c and f) were used to further understand the optoelectronic and photophysical properties of our carotenoid-based polymers. We characterized the chemical

doping, oxidation and degradation of caro-PPV and p(CP-hexyl) *via* electron paramagnetic resonance (EPR) and UV-Vis using FeCl$_3$ and trifluoroacetic acid (TFA) as dopants. Lastly, electronic performances of pristine and doped polymers were assessed from charge carrier mobility measurements of thin-film organic field-effect transistors (OFETs). Overall, we found that caro-PPV performed substantially better than its imine counterpart, with charge carrier mobilities up to four orders of magnitude greater in both the pristine and doped states. These findings provide further motivation to explore carotenoid-based polymers as promising degradable organic semiconductors.

Results and discussion

Synthesis and polymer characterization

Two polymers, caro-PPV and p(CP-hexyl), along with their respective model compounds, were synthesized using the C10 dialdehyde monomer (Fig. 1). The model compounds (Fig. 1c and f) were used to optimize synthetic conditions, and identify characteristic trends for density functional theory (DFT) calculations, photophysical experiments, and chemical doping experiments. The imine model compound and p(CP-hexyl) were prepared *via* imine condensation reactions (Fig. 1a) using the C10 dialdehyde monomer and diamines as previously reported.[17] On the other hand, the non-imine model compound and caro-PPV were synthesized *via* the Horner–Wadsworth–Emmons (HWE) reaction (Fig. 1d). This method was selected due to its compatibility with dialdehyde monomers and its capacity for high yielding polymerizations.[32–36] The HWE monomer was prepared *via* three reactions; a Kumada coupling to install dihexyl side chains, a bromomethylation reaction,[37] followed by a Michaelis–Arbuzov reaction to install bisphosphonate esters. Detailed synthetic procedures and characterization for all model compounds, monomers and polymers are found in the ESI (Fig. S1–33 and Tables S1–S6†).

Polymerization conditions for both caro-PPV and p(CP-hexyl) were optimized to yield low molecular weight polymers for ease of characterization and maximal solubility. Gel permeation chromatography (GPC) yielded a number average molecular weight M_n under 4000 g mol^{-1} for each polymer with comparable degrees of polymerization (DP) (Table 1). The

polymers were further characterized using ^{1}H NMR, with small differences noted between the polymers (*i.e.* imine bond peak in p(CP-hexyl)). Additionally, we observed minor unidentified peaks in the ^{1}H NMR spectra of caro-PPV, which we attribute to oxidation as carotenoids are known to be susceptible to oxidation over time[29–31] (Fig. S31†). However, no observable changes were noted in the GPC traces over time, suggesting that the oxidation of caro-PPV from ambient conditions does not cause depolymerization of the main chain. In contrast, p(CP-hexyl) was more stable, being stored at −20 °C in ambient conditions over extended periods of time.

Optoelectronic properties

The optoelectronic properties of both model compounds and polymers were studied using ultraviolet-visible (UV-Vis) spectroscopy (Fig. 2) with chloroform as the solvent in solution state and chlorobenzene for spin-coated thin films. Solution studies of the non-imine model compound revealed three distinct maxima (Fig. 2a), which is attributed to the S$_0$–S$_2$ transition, a characteristic observed for carotenoid molecules.[38] The polymer counterpart, caro-PPV, has a single maximum, with a red-shifted absorbance maximum (λ_{max}) at 491 nm in solution, and 470 nm in thin film (Table 2). The disappearance of the three distinct peaks in the polymer spectrum is attributed to an increase in conjugation length and increased disorder between carotenoid units, leading to peak broadening. Caro-PPV exhibited a lower λ_{max} in the thin film state compared to in solution and a red-shifted absorption onset (λ_{onset}), for which we attribute to polymer aggregation and points to a more complex electronic structure[39] in the solid-state compared to the solution-state.

In contrast to caro-PPV, p(CP-hexyl) and the imine model compound exhibited a lower λ_{max} and λ_{onset} in all conditions (Fig. 2b). For the imine model compound, we observed a disappearance of the S$_0$–S$_2$ transition, which we suspect arises from increased electronic disorder due to geometric and solvation effects of the imine bond. The p(CP-hexyl) polymer in both solution and thin film measurement features a double peak, which was not observed with caro-PPV. As such, we associate the lower wavelength peak to an n–π* transition arising from the C=N bonds in the polymer backbone of p(CP-hexyl). However, since p(CP-hexyl) is less conjugated compared to caro-PPV (DP of 8 instead of 9), we cannot ignore that conjugation length is also a factor to the lower λ_{max} observed in both the solution and thin film measurements. We observed a blue-shift in the peak absorbance in the solid state for p(CP-hexyl), along with a slight red-shift of the absorption edge and reduction in the 0–0/0–1 peak ratio. Although the vibronic structure cannot be resolved in caro-PPV, we detect similar slight spectral broadening, rebalancing of the spectral shape, and peak blue-shift in solid-state. These characteristics are typical of weakly coupled H-aggregates,[40] and the spectral changes are similar to earlier reports of H-aggregates carotenoid aggregates.[39] Further, cyclic voltammetry was used to probe electrochemical differences between imine and non-imine model compounds and polymers

Table 1 Summary of GPC characterization of carotenoid-based polymers

Polymer	M_n (g mol^{-1})	M_w (g mol^{-1})	Đ	DP[a]
Caro-PPV	3720	5390	1.4	9
p(CP-hexyl)[b]	3550	8075	2.3	8

[a] The degree of polymerization (DP) was calculated from M_n obtained from GPC (solvent: THF, 40 °C, relative to polystyrene standards). [b] The values of the bimodal peak distribution are summarized in this table (see Fig. S29†).

Fig. 2 Optoelectronic characterization of carotenoid-based model compounds and polymers. (a) UV-Vis absorption spectra of the non-imine model compound in solution in chloroform, and caro-PPV in thin film (chlorobenzene) and solution (chloroform) state. (b) UV-Vis absorption spectra of the imine model compound in solution in chloroform, and p(CP-hexyl) in thin film (chlorobenzene) and solution (chloroform) state. (c) HOMO and LUMO energy levels determined from DFT calculations for the two model compounds and two polymers.

(Fig. S44†). Both model compounds exhibited two major oxidation peaks, whereas the polymers exhibited 1 major oxidation peak. In general, the non-imine model compound and caro-PPV exhibited quasi-reversible oxidation, whereas the imine model compound and p(CP-hexyl) demonstrated irreversible oxidation, with subsequent scans leading to complete degradation.

To better understand the impact of the imine bond on the optoelectronic properties of carotenoid-based polymers, density functional theory (DFT) and time-dependent DFT (TDDFT) studies were performed. Specifically, the optimized ground-state structures and singlet-excited states of the model compounds and polymers were investigated (see ESI† for computational details). The imine model compound showed reduced planarity due to a higher torsional strain between the phenyl group and the imine bond with a dihedral angle, ψ, of 40.1° compared to 2.8° for the non-imine compound (Fig. S34†). The high torsional distortion of the imine compound is likely due to steric strain imposed by the phenyl group, as the thiophene analogue reported in literature by Bao and coworkers[25] was planar. The optimized DFT geometry of the imine model compound aligned well with X-ray crystallographic results (Tables S1–S6†). For the imine and non-imine compounds, TDDFT calculations showed the first singlet-excited state involves the HOMO to LUMO transition as the dominant contributors. The imine bond lowers the LUMO energy because of its electron-withdrawing effects, with an observed greater reduction in the HOMO level based on our calculations. However, we acknowledge that the HOMO level results are likely not an accurate representation as polyenes are notoriously difficult to model and would require multireference methods to validate, particularly regarding the correct energy ordering of the lowest bright and dark singlet-excited states. Nevertheless, the imine model compound results in a larger calculated HOMO–LUMO gap (5.46 eV vs. 5.04 eV) and a lower theoretical λ_{max} (408 nm vs. 386 nm) compared to the non-imine model (Fig. S35 and S36†).

The computational trends of p(CP-hexyl) and caro-PPV are consistent with the observation for their model compounds. Greater torsional distortion was observed in the p(CP-hexyl) than caro-PPV along the polymer axis with a dihedral angle (ψ) of 42.2° and 22.2°, respectively (Fig. S37†). However, unlike the model compounds, the first singlet-excited state of p(CP-hexyl) is primarily characterized by the HOMO−1 to LUMO transition, whereas for caro-PPV, it is dominated by the HOMO to

Table 2 Summary of optoelectronic properties of carotenoid-based polymers

Polymer	Solution						Thin film	
	λ_{max}^{sol} (nm)	λ_{onset}^{sol} [a] (nm)	E_g^{sol} [b] (eV)	E_{HOMO} [c] (eV)	E_{LUMO} [c] (eV)	λ_{max}^{film} (nm)	λ_{onset}^{film} [a] (nm)	E_g^{film} [d] (eV)
Caro-PPV	491	575	4.59	−6.10	−1.51	470	584	2.12
p(CP-hexyl)	473	560	4.82	−6.41	−1.59	458	582	2.13

[a] λ_{onset} calculated using onset program.[64] [b] E_g^{sol} was calculated from E_{HOMO} and E_{LUMO}. [c] E_{HOMO} and E_{LUMO} were obtained from DFT calculations. [d] E_g^{film} was calculated from λ_{onset}^{film}.

LUMO transition (Fig. 1b, e, and Fig. S38†). Since multiple transitions with differing contributions are involved, natural transition orbitals (NTO) were computed for the polymers to understand their photophysical properties. Caro-PPV exhibits greater electron delocalization in its highest-occupied NTO (HONTO) and conjugation in its lowest-unoccupied NTO (LUNTO) compared to p(CP-hexyl), resulting in a higher theoretical λ_{max} of 451 nm *versus* 417 nm, respectively (Fig. S39 and S40†). The planarity and steric effects imposed by the imine bond (−C═N−) compared to the vinylene group (−C═C−) were investigated by rotational barrier analysis where ψ is rotated from 0–360° on methyl-appended model compounds (Fig. S41†). The imine model experiences a higher rotational barrier than the non-imine model. Unlike the non-imine model, where the barrier is highest when $\psi = 90°$, the imine model exhibits the highest barrier when $\psi = 180°$ due to the steric strain occurring between the phenyl group and the imine hydrogen. In contrast, the steric strain in the non-imine model when $\psi = 180°$ is ~3.5 kcal mol^{-1} lower. In summary, because of the smaller torsional distortion along the polymer backbone of caro-PPV, it exhibits greater planarity and higher effective conjugation, which contributes to the observed difference in optoelectronic properties.

Photophysical properties

Motivated by the widespread interest in the ultrafast excited-state relaxation dynamics of carotenoids,[39,41–44] we sought to study the femtosecond resolved photophysics of our carotenoid-based polymers and corresponding model compounds using solution-phase transient absorption (TA) spectroscopy. In these pump–probe measurements, we tracked changes in the sample's absorption of white light due to the presence of photoexcited states, as a function of time delay after the excitation pulse, with a temporal resolution of either ~200 fs (selective, narrowband excitation) or ~10 fs (broadband excitation). Different electronic states were identified by signature combinations of three types of feature: ground-state bleaching (GSB) with $\Delta T/T > 0$, reflecting depletion of the molecular ground-state absorption; stimulated emission (SE) with $\Delta T/T > 0$, which tracks the molecular photoluminescence; and photo-induced absorption (PIA) with $\Delta T/T < 0$, which reveals absorption transitions to higher states within the excited manifold. In polyenes, TA measurements have firmly established a basic three-state relaxation scheme.[45] Excitation of the bright second excited state S_2 is followed by internal conversion to the dark first excited state S_1, typically on ultrafast timescales suggesting a conical intersection. The S_1 state is also short-lived, exhibiting rapid non-radiative decay back to S_0.

Our TA measurements in Fig. 3 indicate that both polymers follow this polyene framework, and we observe similar behaviour in the model compounds (Fig. S45†).[41] Both polymers have similar excited-state features, with the foremost difference being that caro-PPV exhibits slower relaxation dynamics compared to p(CP-hexyl). The primary features in caro-PPV are the GSB at 475 nm and a strong PIA at 710 nm. We assigned the latter to the initial excitation S_2, and it rapidly decayed simul-

Fig. 3 Femtosecond time-resolved transient absorption data of (a) caro-PPV and (b) p(CP-hexyl) polymers prepared in chlorobenzene solution. Both caro-PPV and p(CP-hexyl) were pumped at 460 nm, with temporal resolution <200 fs and a laser power of 400 μW.

taneously with the appearance of a new PIA at 575 nm. The latter is the longest-lived signal, and its appearance coincides with a blue-shift of the $\Delta T/T > 0$ band which we attribute to a disappearance of SE from S_2. Accordingly, we assign the second PIA to the dark S_1 state and find an internal conversion time-constant of <1 ps. Analogous characteristic bands are observed in p(CP-hexyl) (Fig. 3b), namely GSB at 460 nm, an initial (S_2) PIA at 725 nm and a longer-lived (S_1) PIA at 550 nm. Unlike in caro-PPV, using 200 fs, narrowband excitation we can detect no sign of SE from S_2 in the imine polymer. However, when we perform the equivalent experiment with higher resolution using 10 fs, broadband pump pulses, we observe clear SE from S_2 at ~525 nm, as shown at a 40 fs pump–probe delay in Fig. 3b. The S_2–S_1 internal conversion is especially rapid in the imine polymer, with kinetic fitting revealing an initial time-constant of ~18 fs (Fig. S46†). Extracted kinetics and TA measurements on model compounds and polymers are presented in more detail in the ESI (Fig. S45–47 and Table S7†).

By observing the general photophysics of these carotenoid-based polymers and model compounds, we note that the imine-based polymer and monomer have significantly faster kinetics compared to their non-imine counterparts, both for S_2–S_1 internal conversion and ultimate relaxation to the

ground state. The carotenoid-based polymers also have faster lifetimes compared to their model compound analogues, which is common in polyenes as the degree of polymerization, and hence π-conjugation, increases.[46]

Additional narrowband TA studies were performed to understand the effects of doping on the electronic properties of the carotenoid-based polymers. Here, we use the ability to generate polarons through photoinduced charge-transfer to an electron acceptor as a proxy for the ease of doping (see below). The fullerene derivative, phenyl-C_{61}-butyric acid methyl ester (PCBM), is a common acceptor used as a dopant to enable polaron formation in an active material.[47] To study these effects, we prepared polymer-PCBM blend films by spin-coating onto quartz-coated substrates. The films were prepared in an inert atmosphere and encapsulated to prevent photochemical degradation. We probed the charge-transfer dynamics in TA as shown in Fig. 4. Both polymer films had similar GSB and PIA features compared to the solution-phase studies described above. For caro-PPV films (Fig. 4a), doping with increasing weight percentage (wt%) of PCBM resulted in a new, broad, long-lived PIA that persisted past the 7 ns limit of our delay stage. This new signature is characteristic of a polaron and gives us a deeper insight to the different charge separation abilities between the two polymers. Namely, in the p(CP-hexyl) film, the same two distinct PIA peaks previously observed in solution (Fig. 3) were preserved across all doped

films with no new evidence of any additional states. However, we note that the decay kinetics of p(CP-hexyl) are progressively slowed with increasing PCBM wt% (Fig. S48†). Overall, caro-PPV was found to be notably more efficient at photogenerating charges compared to p(CP-hexyl).

Chemical doping & degradation studies

Following the optoelectronic and photophysical characterization of our carotenoid-based polymers, we examined the effect of chemical doping and polymer degradation using two p-type dopants: $FeCl_3$ and trifluoroacetic acid (TFA). These chemical dopants were selected for their ability to (1) dope carotenoid molecules *via* redox or Lewis-acid mechanisms,[48–51] (2) improve the conductivity of organic semiconductors[27,52–54] and (3) degrade carotenoids *via* radical mechanisms.[29–31] First, we investigated the effect of $FeCl_3$ and TFA on the optical properties of caro-PPV (Fig. 5a and b) using solution-state UV-Vis spectroscopy. Compounds were dissolved in chloroform for $FeCl_3$ doping studies and chlorobenzene for TFA doping studies, with all studies conducted in ambient conditions without the use of anhydrous solvents. Firstly, in $FeCl_3$ doping studies, caro-PPV experienced a decrease in absorbance at its λ_{max} (491 nm), with a gradual shift to shorter wavelengths (Fig. 5a) accompanied by a colour change from red to green. Notably, a broad peak spanning 800–1400 nm appeared with increasing $FeCl_3$ concentrations, which we attribute to the for-
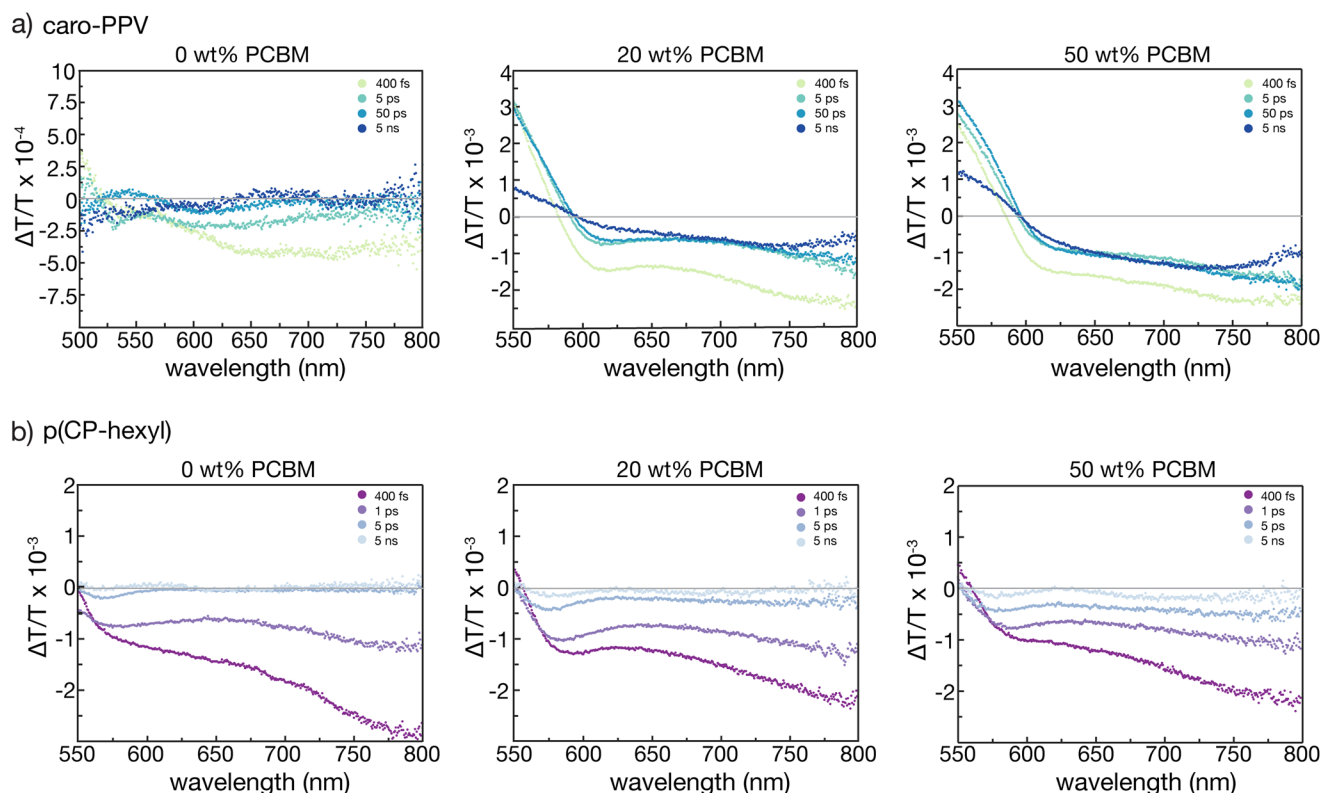

Fig. 4 Femtosecond time-resolved transient absorption graphs represented in terms of $\Delta T/T$ of PCBM doped films (0, 20, 50 wt%) of (a) caro-PPV and (b) p(CP-hexyl) polymers. Both caro-PPV and p(CP-hexyl) were pumped at 460 nm, with temporal resolution <200 fs and a laser power of 400 μW.

Fig. 5 Chemical doping studies of caro-PPV and p(CP-hexyl) polymers. (a) caro-PPV (0.02 mg mL^{-1}) consecutively doped with varying concentrations of FeCl$_3$ solution in chloroform. Inset shows solution colour change upon chemical doping. (b) caro-PPV (0.02 mg mL^{-1}) consecutively doped with varying concentrations of TFA solution in chlorobenzene. Inset shows solution colour change upon chemical doping. (c) Overlay of EPR spectra for caro-PPV (2 mg mL^{-1}) in the pristine, FeCl$_3$ (1 mM) and TFA (50 mM) - doped states. (d) p(CP-hexyl) (0.02 mg mL^{-1}) consecutively doped with varying concentrations of FeCl$_3$ solution in chloroform. Inset shows solution colour change upon chemical doping. (e) p(CP-hexyl) (0.02 mg mL^{-1}) consecutively doped with varying concentrations of TFA solution in chlorobenzene. Inset shows solution colour change upon chemical doping. (f) overlay of EPR spectra for p(CP-hexyl) (2 mg mL^{-1}) in the pristine, FeCl$_3$ (0.5 mM) and TFA (0.5 mM) − doped states.

mation of radicals across the polymer backbone. A similar trend was observed with caro-PPV with increasing concentrations of TFA (Fig. 5b), in which the λ_{max} (491 nm) shifts to a shorter wavelength and decreases in absorbance, and a new broad peak appears at 800–1400 nm. These findings are consistent with literature reports on the acid-doping of β-carotene, for which the red-shifted peak is associated with the formation of short-lived radical carbocations.[49]

To evaluate our hypothesis regarding the formation of radicals, electron paramagnetic resonance (EPR) was used. To observe short-lived radicals, 5,5-dimethyl-1-pyrroline N-oxide (DMPO) was used as a spin trap. In the absence of a dopant, there was no observable EPR signal for pristine caro-PPV mixed with DMPO (Fig. 5c). Addition of FeCl$_3$ or TFA produced a four-line EPR spectrum with a splitting pattern that is characteristic of the DMPO-OOH spin adduct.[55,56] The formation of the DMPO-OOH spin adduct is indicative of successful doping of caro-PPV in the presence of FeCl$_3$ or TFA, generating O$_2$$^{•-}$ radicals *in situ*. Similar results were obtained when the experiments were performed on the non-imine model com-

pound (Fig. S49–50 and 56†), aligning well with previous reports on other carotenoid small molecules.[49,50,57,58] Overall, our observations suggest that the carotenoid moiety in caro-PPV's backbone is a driving factor for the chemical doping behaviours with FeCl$_3$ and TFA.

Unlike caro-PPV, which showed a broad absorption peak in the UV-vis spectra upon FeCl$_3$ and TFA addition, p(CP-hexyl) exhibited different spectral changes under the same conditions. Adding FeCl$_3$ to p(CP-hexyl) led to the formation of a new λ_{max} at 556 nm (Fig. 5d) alongside a colour change from orange to purple. These findings are consistent with previously reported poly(azomethine)s, which form radical cations in the presence of a one-electron oxidant such as FeCl$_3$.[53,59] As observed with caro-PPV, the EPR spectra of doped p(CP-hexyl) featured a four-line signal consistent with a DMPO spin adduct (Fig. 5f), confirming the presence of newly formed radical species. Moreover, the FeCl$_3$ doping effects for the imine model and p(CP-hexyl) were further investigated using DFT and TDDFT calculations where we propose that that FeCl$_3$ behaves like a Lewis acid and coordinates to the imine func-

tional group (Fig. S42 and 43†). At the theoretical λ_{max} of 442 nm, which corresponds to the 4th singlet-excited state, two dominant NTO pairs are involved – the HONTO and LONTO of each α- and β-spin orbitals. The α- and β-spin orbitals pairs indicate a strong π–π* transition of the imine model backbone and strong ligand-to-metal-charge transfer of the chloride atoms to the iron centre, respectively.

When p(CP-hexyl) was treated with TFA, there was an initial decrease in absorbance at its λ_{max}, followed by the appearance of two peaks (one red-shifted and the other blue-shifted) (Fig. 5e). At sufficiently high TFA concentrations (>100 mM), a single, blue-shifted maximum is observed. The red-shifted maximum is associated with the protonated state of p(CP-hexyl), which is commonly observed for poly(azomethine)s in the presence of TFA.[12,16,60] However, the observed protonated peak disappears at higher concentrations of TFA, resulting in a single blue-shift, suggesting fragmentation of the polymer into oligomeric units. Furthermore, the EPR spectrum of p(CP-hexyl) with TFA confirmed the formation of radical species, with the distinct four-peak signal corresponding to the DMPO-OOH spin adduct observed, comparable to caro-PPV (Fig. 5f and S56†).

Chemical doping in the solid-state was also investigated for both caro-PPV and p(CP-hexyl) by placing thin films (spin-coated with chlorobenzene) in a sealed container with dopants for various amounts of time and monitoring spectral changes *via* UV-Vis spectroscopy (Fig. S50†). When studying caro-PPV in the solid state, we observed a decrease in λ_{max} upon longer exposure to both FeCl$_3$ or TFA vapours (Fig. S50a and b†). In contrast, we observed a red-shifted λ_{onset} upon longer exposure to both FeCl$_3$ or TFA (Fig. S50c and d†) for p(CP-hexyl). These observations suggest chemical doping of caro-PPV occurs more readily when the polymer is dissolved in solution rather than in the solid state. This observation is consistent with Araujo, Wang and colleagues[61] in which they observed differences in the acidochromic behaviour of vinyl *versus* imine bonds in the solid state compared to solution state.

The oxidative degradation of both polymers using FeCl$_3$ and TFA was subsequently investigated. For caro-PPV exposed to FeCl$_3$ in solution, the doped state disappeared after 48 hours, followed by a blue-shift in the main polymer chain absorbance peak (Fig. S51a, b and c†). However, degradation occurred more rapidly with p(CP-hexyl) in the presence of FeCl$_3$, with the characteristic C10 dialdehyde peak[17] dominating the UV-Vis spectrum after a 24 hour period (Fig. S51c, d and e†). These notable differences in degradation between caro-PPV and p(CP-hexyl) provides evidence that the FeCl$_3$ doping mechanism differs between these two polymers. We hypothesize that when the imine bond is present, hydrolysis may still occur at the imine bond due to the *in situ* production of HCl from FeCl$_3$ over time, resulting in C10 dialdehyde as a predominant byproduct. Contrarily, without an imine bond present in the polymer, FeCl$_3$ oxidation occurs broadly along the conjugated backbone, such that C10 dialdehyde is no longer the predominant byproduct produced.

The reversibility of chemical doping in solution for both caro-PPV and p(CP-hexyl) was investigated. To study the rever-

sibility of doping with FeCl$_3$, hydrazine was added to prepared doped solutions (Fig. S53†). For both polymers, doping was reversible as indicated by a return to pristine λ_{max} values accompanied by a change to the original solution colour. To study the reversibility of doping with TFA, triethylamine was added to prepared doped solution (Fig. S54†). With caro-PPV, we observed reversible doping, with the λ_{max} returning to pristine polymer absorbance levels (Fig. S54a, b and c†). However, reversibility was not observed with p(CP-hexyl), where degradation persisted despite the addition of triethylamine and the characteristic C10 dialdehyde peak was yet again observed (Fig. S54d, e and f†). This demonstrates the fragility of the imine bond in this polymer system, and emphasizes that protonation, followed by imine bond cleavage, occurs so rapidly that it cannot be reversed. It should be noted that degradation is still inevitable with caro-PPV if left in solution with TFA for several hours (Fig. S55†) as we observed the λ_{max} peak gradually blue-shift and the disappearance of the doping peak. This is consistent with the degradation of carotenoid small molecules into peroxides and carotenyl trifluoroacetate byproducts in the presence of TFA under ambient conditions.[49] These studies show that our caro-PPV polymer degrades under acidic conditions without the presence of an imine bond, creating opportunities for future investigation of acid-based degradation methods using this moiety.

Organic field-effect transistors

To understand the effect of chemical doping on the electronic performance of carotenoid-based polymers, bottom-gate top-contact organic field-effect transistors (OFETs) were fabricated using octadecyl trimethoxy silane (OTS)-modified SiO$_2$ as the dielectric, highly doped Si as the gate, Au electrodes, and caro-PPV or p(CP-hexyl) as the semiconducting layer (Fig. 6a). Transfer curves for pristine and doped caro-PPV are represented in Fig. 6b, with representative transfer and output curves for all pristine and doped polymers available in the ESI (Fig. S57 and 58†). The average performance metrics for all OFETs are summarized in Table 3, with the average charge carrier mobility (μ_{avg}) graphically represented in Fig. 6c.

As with our previous chemical doping study, FeCl$_3$ was used as one of the dopants, while *p*-toluenesulfonic acid (PTSA), was selected over TFA for easier device fabrication. All polymers were prepared in chlorobenzene, with dopants added in solution prior to spin coating onto prepared wafers (see ESI†). OFETs of pristine and doped caro-PPV exhibited ambipolar charge transport under nitrogen with dominant p-type behaviour. Mobilities were extracted from the saturation regime, with pristine caro-PPV and PTSA-doped caro-PPV performing the best with mobilities on the order of 10^{-4} cm^2 V^{-1} s^{-1}. Caro-PPV doped with FeCl$_3$ experienced a slight decrease in mobility compared to the pristine polymer, on the order of 10^{-5} cm^2 V^{-1} s^{-1}. In contrast, p(CP-hexyl) performed poorly, with mobilities on the order of 10^{-8} cm^2 V^{-1} s^{-1}, regardless of the presence of dopants. The performance of p(CP-hexyl) is on par with the electronic performance of β-carotene reported in similar device architectures,[62,63] which further demonstrates

Fig. 6 Electronic performance of carotenoid-based OFETs. (a) Bottom-gate top-contact (BGTC) device architecture used. (b) Representative saturation transfer curves for caro-PPV polymer under doped conditions ($V_{DS} = -100$ V). The dashed lines correspond to the square root of the drain current. (c) Average charge carrier mobilities (extracted from up and down transfer curves) from 10 devices of caro-PPV and p(CP-hexyl)-doped polymers.

Table 3 OFET parameters of carotenoid-based polymers under vacuum condition

	$\mu_{avg} \times 10^{-5}$ [cm^2 V^{-1} s^{-1}]^a	I_{on}/I_{off}	V_T [V]
Caro-PPV	14 ± 6.0	10^2–10^3	-35 ± 17
Caro-PPV + FeCl$_3$	5.6 ± 4.9	10^2–10^3	-32 ± 17
Caro-PPV + PTSA	18 ± 7.3	10^2–10^3	-47 ± 17
p(CP-hexyl)	0.0054 ± 0.007	10^1	4 ± 300
p(CP-hexyl) + FeCl$_3$	0.0098 ± 0.006	10^1	83 ± 350
p(CP-hexyl) + PTSA	0.0022 ± 0.002	10^1	212 ± 70

^{a} μ_{avg} calculated from a minimum of 10 devices across 3 chips.

the detrimental effect of the imine bond on electronic performance despite the increase of conjugation length in the polymeric state. We note that the transfer and output curves for p(CP-hexyl) and some of the output curves for caro-PPV are non-standard and we attribute this to poor semiconductor performance, as seen with β-carotene.[62]

Overall, while the molecular design of caro-PPV greatly increased the mobility of carotenoid-based polymers by four orders of magnitude, further exploration is needed to improve on the electronic properties of carotenoid-based polymers. As the polymers in this study were of low molecular weight (<4 kg mol^{-1}) compared to most high-performing semiconducting polymers (>20 kg mol^{-1}), synthesizing higher molecular weight caro-PPV and exploring other monomeric designs that reduce torsional distortions may improve overall mobility.

Conclusions

Carotenoid-based polymers offer much promise for degradable conjugated polymers and can be synthetically modified to improve electronic properties. In this study, we characterized the optoelectronic and photophysical properties, chemical doping, degradation and OFET performance of two carotenoid-based polymers: caro-PPV and p(CP-hexyl). Specifically, we evaluated the effect of imine bonds on electronic properties of carotenoid-based polymers. We found that caro-PPV, our polymer without imine bonds, had higher charge carrier mobilities compared to our imine variant, p(CP-hexyl). While there is room to improve the charge carrier mobility values, the results of this study indicate positive steps towards the development of carotenoid-based polymers for applications in degradable electronics.

Author contributions

All authors have given approval to the final version of the manuscript. Conceptualization, A.U., H.T., A.J.M.; synthesis and characterization of model compounds, monomers, polymers, UV-Vis studies, EPR, OFET fabrication, CV, data analysis, manuscript writing, A.U.; transient absorption spectroscopy, data analysis, writing, Y.K.; polymer synthesis, OFET optimizations, data analysis, S.M.; DFT calculations, data analysis, N.S.Y.H.; ultrafast transient absorption spectroscopy, D.C.B.; OFET optimizations, S.H.H.; editing, all authors.

Data availability

The data supporting this article has been included as part of the ESI.†

Conflicts of interest

There are no conflicts to declare.

Acknowledgements

References

1 M. Wang, P. Baek, A. Akbarinejad, D. Barker and J. Travas-Sejdic, Conjugated Polymers and Composites for Stretchable Organic Electronics, *J. Mater. Chem. C*, 2019, **7**(19), 5534–5552.

2 J. Xu, H.-C. Wu, J. Mun, R. Ning, W. Wang, G.-J. N. Wang, S. Nikzad, H. Yan, X. Gu, S. Luo, D. Zhou, J. B.-H. Tok and Z. Bao, Tuning Conjugated Polymer Chain Packing for Stretchable Semiconductors, *Adv. Mater.*, 2022, **34**(22), 2104747.

3 M. Ashizawa, Y. Zheng, H. Tran and Z. Bao, Intrinsically Stretchable Conjugated Polymer Semiconductors in Field Effect Transistors, *Prog. Polym. Sci.*, 2020, **100**, 101181.

4 Y. Xu, X. Wang, J. Zhou, B. Song, Z. Jiang, E. M. Y. Lee, S. Huberman, K. K. Gleason and G. Chen, Molecular Engineered Conjugated Polymer with High Thermal Conductivity, *Sci. Adv.*, 2018, **4**(3), eaar3031.

5 X. Rodríguez-Martínez, F. Saiz, B. Dörling, S. Marina, J. Guo, K. Xu, H. Chen, J. Martin, I. McCulloch, R. Rurali, J. S. Reparaz and M. Campoy-Quiles, On The Thermal Conductivity of Conjugated Polymers for Thermoelectrics, *Adv. Energy Mater.*, 2024, **14**(35), 2401705.

6 V. R. Feig, H. Tran and Z. Bao, Biodegradable Polymeric Materials in Degradable Electronic Devices, *ACS Cent. Sci.*, 2018, **4**(3), 337–348.

7 J. Tropp and J. Rivnay, Design of Biodegradable and Biocompatible Conjugated Polymers for Bioelectronics, *J. Mater. Chem. C*, 2021, **9**(39), 13543–13556.

8 A. Uva, S. Michailovich, N. S. Y. Hsu and H. Tran, Degradable π-Conjugated Polymers, *J. Am. Chem. Soc.*, 2024, **146**(18), 12271–12287.

9 T. Lei, X. Chen, G. Pitner, H. S. P. Wong and Z. Bao, Removable and Recyclable Conjugated Polymers for Highly Selective and High-Yield Dispersion and Release of Low-Cost Carbon Nanotubes, *J. Am. Chem. Soc.*, 2016, **138**(3), 802–805.

10 H. Jin, K. K. Kim, S. Park, J. H. Rhee, H. Ahn, D. J. Kim, K. K. Kim, J. H. Noh, T. S. Kim, E. Y. Shin and H. J. Son, Chemically Recyclable Conjugated Polymer and One-Shot Preparation of Thermally Stable and Efficient Bulk-Heterojunction from Recycled Monomer, *Adv. Funct. Mater.*, 2023, 2304930.

11 N. Nozaki, A. Uva, H. Matsumoto, H. Tran and M. Ashizawa, Thienoisoindigo-Based Recyclable Conjugated Polymers for Organic Electronics, *RSC Appl. Polym.*, 2024, **1**(2), 163–171.

12 A. Charland-Martin and G. S. Collier, Understanding Degradation Dynamics of Azomethine-Containing Conjugated Polymers, *Macromolecules*, 2024, **57**(13), 6146–6155.

13 K. A. Bartlett, A. Charland-Martin, J. Lawton, A. L. Tomlinson and G. S. Collier, Azomethine-Containing Pyrrolo[3,2-b]Pyrrole Copolymers for Simple and Degradable Conjugated Polymers, *Macromol. Rapid Commun.*, 2023, **45**, 2300220.

14 J. A. Chiong, Y. Zheng, S. Zhang, G. Ma, Y. Wu, G. Ngaruka, Y. Lin, X. Gu and Z. Bao, Impact of Molecular Design on Degradation Lifetimes of Degradable Imine-Based Semiconducting Polymers, *J. Am. Chem. Soc.*, 2022, **144**(8), 3717–3726.

15 J. A. Chiong, L. Michalek, A. E. Peña-Alcántara, X. Ji, N. J. Schuster and Z. Bao, Degradable Semiconducting Polymers without Long-Range Order for on-Demand Degradation of Transient Electronics, *J. Mater. Chem. C*, 2023, **11**(43), 15205–15214.

16 N. Nozaki, A. Uva, T. Iwahashi, H. Matsumoto, H. Tran and M. Ashizawa, Impact of Aromatic to Quinoidal Transformation on the Degradation Kinetics of Imine-Based Semiconducting Polymers, *RSC Appl. Polym.*, 2025, **3**, 257–267.

17 A. Uva, A. Lin and H. Tran, Biobased, Degradable, and Conjugated Poly(Azomethine)s, *J. Am. Chem. Soc.*, 2023, **145**(6), 3606–3614.

18 M. H. Liang, Y. J. He, D. M. Liu and J. G. Jiang, Regulation of Carotenoid Degradation and Production of Apocarotenoids in Natural and Engineered Organisms, *Crit. Rev. Biotechnol.*, 2021, **41**(4), 513–534.

19 M. J. Llansola-Portoles, A. A. Pascal and B. Robert, Electronic and Vibrational Properties of Carotenoids: From in Vitro to in Vivo, *J. R. Soc. Interface*, 2017, **14**, 20170504.

20 A. Singh and T. Mukherjee, Application of Carotenoids in Sustainable Energy and Green Electronics, *Mater. Adv.*, 2022, **3**(3), 1341–1358.

21 Y. Zhao, S. Lindsay, S. Jeon, H. J. Kim, L. Su, B. Lim and S. Koo, Combined Effect of Polar Substituents on the Electronic Flows in the Carotenoid Molecular Wires, *Chem. – Eur. J.*, 2013, **19**(33), 10832–10835.

22 R. C. Mordi, Mechanism of Beta-Carotene Degradation, *Biochem. J.*, 1993, **292**(Pt 1), 310.

23 M. H. Walter and D. Strack, Carotenoids and Their Cleavage Products: Biosynthesis and Functions, *Nat. Prod. Rep.*, 2011, **28**(4), 663–692.

24 C. I. Cazzonelli, Carotenoids in Nature: Insights from Plants and Beyond, *Funct. Plant Biol.*, 2011, **38**(11), 833–847.

25 H. Tran, S. Nikzad, J. A. Chiong, N. J. Schuster, A. E. Peña-Alcántara, V. R. Feig, Y.-Q. Q. Zheng and Z. Bao, Modular Synthesis of Fully Degradable Imine-Based Semiconducting p-Type and n-Type Polymers, *Chem. Mater.*, 2021, **33**(18), 7465–7474.

26 F. C. Krebs and M. Jørgensen, High Carrier Mobility in a Series of New Semiconducting PPV-Type Polymers, *Macromolecules*, 2003, **36**(12), 4374–4384.

27 M. Tzolov, V. P. Koch, W. Bruetting and M. Schwoerer, Optical Characterization of Chemically Doped Thin Films of Poly(p-Phenylene Vinylene), *Synth. Met.*, 2000, **109**(1–3), 85–89.

28 T. Lei, J. H. Dou, X. Y. Cao, J. Y. Wang and J. Pei, Electron-Deficient Poly(p-Phenylene Vinylene) Provides Electron Mobility over 1 Cm2 V-1 s-1 under Ambient Conditions, *J. Am. Chem. Soc.*, 2013, **135**(33), 12168–12171.

29 F. Ramel, A. S. Mialoundama and M. Havaux, Nonenzymic Carotenoid Oxidation and Photooxidative Stress Signalling in Plants, *J. Exp. Bot.*, 2013, **64**(3), 799–805.

30 F. Ramel, S. Birtic, C. Ginies, L. Soubigou-Taconnat, C. Triantaphylidès and M. Havaux, Carotenoid Oxidation Products Are Stress Signals That Mediate Gene Responses to Singlet Oxygen in Plants, *Proc. Natl. Acad. Sci. U. S. A.*, 2012, **109**(14), 5535–5540.

31 M. Havaux, Carotenoid Oxidation Products as Stress Signals in Plants, *Plant J.*, 2014, **79**(4), 597–606.

32 Z. A. Page, Y. Liu, E. Puodziukynaite, T. P. Russell and T. Emrick, Hydrophilic Conjugated Polymers Prepared by Aqueous Horner-Wadsworth-Emmons Coupling, *Macromolecules*, 2016, **49**(7), 2526–2532.

33 Y. He, W. Ma, N. Yang, F. Liu, Y. Chen, H. Liu and X. Zhu, Efficient Synthesis of Vinylene-Linked Conjugated Porous Networks via the Horner-Wadsworth-Emmons Reaction for Photocatalytic Hydrogen Evolution, *Chem. Commun.*, 2021, **57**, 7557.

34 P. Anuragudom, S. S. Newaz, S. Phanichphant and T. R. Lee, Facile Horner-Emmons Synthesis of Defect-Free Poly(9,9-Dialkylfluorenyl-2, 7-Vinylene), *Macromolecules*, 2006, **39**(10), 3494–3499.

35 C. A. Young, A. Hammack, H. J. Lee, H. Jia, T. Yu, M. D. Marquez, A. C. Jamison, B. E. Gnade and T. R. Lee, Poly(1,4-Phenylene Vinylene) Derivatives with Ether Substituents to Improve Polymer Solubility for Use in Organic Light-Emitting Diode Devices, *ACS Omega*, 2019, **4**(27), 22332–22344.

36 C. A. Young, S. Saowsupa, A. Hammack, A. A. Tangonan, P. Anuragudom, H. Jia, A. C. Jamison, S. Panichphant, B. E. Gnade and T. R. Lee, Synthesis and Characterization of Poly(2,5-Didecyl-1,4-Phenylene Vinylene), Poly(2,5-Didecyloxy-1,4-Phenylene Vinylene), and Their Alternating Copolymer, *J. Appl. Polym. Sci.*, 2014, **131**(23), 41162.

37 A. W. Van der Made and R. H. Van der Made, A Convenient Procedure for Bromomethylation of Aromatic Compounds. Selective Mono-, Bis-, or Trisbromomethylation, *J. Org. Chem.*, 1993, **58**(5), 1262–1263.

38 T. Polívka and V. Sundström, Ultrafast Dynamics of Carotenoid Excited States-from Solution to Natural and Artificial Systems, *Chem. Rev.*, 2004, **104**(4), 2021–2071.

39 A. J. Musser, M. Maiuri, D. Brida, G. Cerullo, R. H. Friend and J. Clark, The Nature of Singlet Exciton Fission in Carotenoid Aggregates, *J. Am. Chem. Soc.*, 2015, **137**(15), 5130–5139.

40 N. J. Hestand and F. C. Spano, Expanded Theory of H- and J-Molecular Aggregates: The Effects of Vibronic Coupling and Intermolecular Charge Transfer, *Chem. Rev.*, 2018, **118**(15), 7069–7163.

41 S. Santra, J. Ray and D. Ghosh, Mechanism of Singlet Fission in Carotenoids from a Polyene Model System, *J. Phys. Chem. Lett.*, 2022, **13**(29), 6800–6805.

42 D. M. Niedzwiedzki, J. O. Sullivan, T. Polívka, R. R. Birge and H. A. Frank, Femtosecond Time-Resolved Transient Absorption Spectroscopy of Xanthophylls, *J. Phys. Chem. B*, 2006, **110**(45), 22872–22885.

43 V. Kuznetsova, M. Fuciman and T. Polívka, Relaxation Dynamics of High-Energy Excited States of Carotenoids Studied by UV Excitation and Pump–Repump–Probe Transient Absorption Spectroscopy, *Phys. Chem. Chem. Phys.*, 2023, **25**(33), 22336–22344.

44 A. Quaranta, A. Krieger-Liszkay, A. A. Pascal, F. Perreau, B. Robert, M. Vengris and M. J. Llansola-Portoles, Singlet Fission in Naturally-Organized Carotenoid Molecules, *Phys. Chem. Chem. Phys.*, 2021, **23**(8), 4768–4776.

45 T. Polívka and V. Sundström, Dark Excited States of Carotenoids: Consensus and Controversy, *Chem. Phys. Lett.*, 2009, **477**(1–3), 1–11.

46 V. Šebelík, M. Kloz, M. Rebarz, M. Přeček, E. H. Kang, T. L. Choi, R. L. Christensen and T. Polívka, Spectroscopy and Excited State Dynamics of Nearly Infinite Polyenes, *Phys. Chem. Chem. Phys.*, 2020, **22**(32), 17867–17879.

47 E. Lioudakis, I. Alexandrou and A. Othonos, Ultrafast Dynamics of Localized and Delocalized Polaron Transitions in P3HT/PCBM Blend Materials: The Effects of PCBM Concentration, *Nanoscale Res. Lett.*, 2009, **4**(12), 1475–1480.

48 G. Gao, Y. Deng and L. D. Kispert, Photoactivated Ferric Chloride Oxidation of Carotenoids by Near-UV to Visible Light, *J. Phys. Chem. B*, 1997, **101**(39), 7844–7849.

49 A. Mortensen and L. H. Skibsted, Kinetics and Mechanism of the Primary Steps of Degradation of Carotenoids by Acid in Homogeneous Solution, *J. Agric. Food Chem.*, 2000, **48**(2), 279–286.

50 L. D. Kispert, T. Konovalova and Y. Gao, Carotenoid Radical Cations and Dications: EPR, Optical, and Electrochemical Studies, *Arch. Biochem. Biophys.*, 2004, **430**(1), 49–60.

51 J. A. Jeevarajan, C. C. Wei, A. S. Jeevarajan and L. D. Kispert, Optical Absorption Spectra of Dications of Carotenoids, *J. Phys. Chem.*, 1996, **100**(14), 5637–5641.

52 T. E. Jones, T. R. Ogden, W. C. McGinnis, W. F. Butler and D. M. Gottfredson, Electronic Properties of Polyacetylene Doped with FeCl$_3$, *J. Chem. Phys.*, 1985, **83**(5), 2532–2537.

53 S. Barik, T. Bletzacker and W. G. Skene, π-Conjugated Fluorescent Azomethine Copolymers: Opto-Electronic, Halochromic, and Doping Properties, *Macromolecules*, 2012, **45**(3), 1165–1173.

54 B. Yurash, D. X. Cao, V. V. Brus, D. Leifert, M. Wang, A. Dixon, M. Seifrid, A. E. Mansour, D. Lungwitz, T. Liu, P. J. Santiago, K. R. Graham, N. Koch, G. C. Bazan and T. Q. Nguyen, Towards Understanding the Doping

Mechanism of Organic Semiconductors by Lewis Acids, *Nat. Mater.*, 2019, **18**(12), 1327–1334.

55 M. Zbyradowski, M. Duda, A. Wisniewska-Becker, Heriyanto, W. Rajwa, J. Fiedor, D. Cvetkovic, M. Pilch and L. Fiedor, Triplet-Driven Chemical Reactivity of β-Carotene and Its Biological Implications, *Nat. Commun.*, 2022, **13**(1), 1–14.

56 F. A. Villamena and J. L. Zweier, Detection of Reactive Oxygen and Nitrogen Species EPR Spin Trapping, *Antioxid. Redox Signal.*, 2004, **6**(3), 619–629.

57 R. C. Mordi, O. T. Ademosun, C. O. Ajanaku, I. O. Olanrewaju and J. C. Walton, Free Radical Mediated Oxidative Degradation of Carotenes and Xanthophylls, *Molecules*, 2020, **25**, 1038.

58 J. L. Grant, V. J. Kramer, R. Ding and L. D. Kispert, Carotenoid Cation Radicals: Electrochemical, Optical, and EPR Study, *J. Am. Chem. Soc.*, 1988, **110**(7), 2151–2157.

59 A. Bolduc, S. Dufresne and W. G. Skene, Chemical Doping of EDOT Azomethine Derivatives: Insight into the Oxidative and Hydrolytic Stability, *J. Mater. Chem.*, 2012, **22**, 5053–5064.

60 N. S. Y. Hsu, A. Lin, A. Uva, S. H. Huang and H. Tran, Direct Arylation Polymerization of Degradable Imine-Based Conjugated Polymers, *Macromolecules*, 2023, **56**(21), 8947–8955.

61 K. Kotewicz, L. R. Franco, M. Araujo and E. Wang, Acidochromic Behaviors of Indacenodithiophene-Based Conjugated Polymers Containing Azo, Imine, and Vinyl Bonds, *Macromolecules*, 2025, **58**(5), 27192729.

62 R. R. Burch, Y. H. Dong, C. Fincher, M. Goldfinger and P. E. Rouviere, Electrical Properties of Polyunsaturated Natural Products: Field Effect Mobility of Carotenoid Polyenes, *Synth. Met.*, 2004, **146**(1), 43–46.

63 M. Irimia-Vladu, P. A. Troshin, M. Reisinger, L. Shmygleva, Y. Kanbur, G. Schwabegger, M. Bodea, R. Schwödiauer, A. Mumyatov, J. W. Fergus, V. F. Razumov, H. Sitter, N. S. Sariciftci and S. Bauer, Biocompatible and Biodegradable Materials for Organic Field-Effect Transistors, *Adv. Funct. Mater.*, 2010, **20**(23), 4069–4076.

64 A. M. Wallace, C. Curiac, J. H. Delcamp and R. C. Fortenberry, Accurate Determination of the Onset Wavelength (Λonset) in Optical Spectroscopy, *J. Quant. Spectrosc. Radiat. Transfer*, 2021, **265**, 107544.